

Crystal Structures and Magnetic Properties of Ordered Perovskites $\text{Ba}_2\text{LnNbO}_6$ ($\text{Ln} = \text{Lanthanide Elements}$)

Kou Henmi and Yukio Hinatsu

Division of Chemistry, Graduate School of Science, Hokkaido University, Sapporo 060-0810, Japan

and

Nobuyuki M. Masaki

Japan Atomic Energy Research Institute, Tokai-mura, Ibaraki 319-1195, Japan

Received March 9, 1999; in revised form June 22, 1999; accepted July 22, 1999

A series of double-perovskite oxides $\text{Ba}_2\text{LnNbO}_6$ ($\text{Ln} = \text{lanthanide elements}$) were synthesized. Their powder X-ray diffraction measurements and Rietveld analysis show that they are monoclinic with space group $P2_1/n$ and that Ln^{3+} and Nb^{5+} ions are structurally ordered. Although the average $\text{Ln}-\text{O}$ bond length increases with the ionic radius of Ln^{3+} , the average $\text{Nb}-\text{O}$ bond length is nearly constant for all the $\text{Ba}_2\text{LnNbO}_6$. Magnetic susceptibility measurements show that they are paramagnetic down to 2 K. The ^{151}Eu Mössbauer spectrum for $\text{Ba}_2\text{EuNbO}_6$ indicates that the Eu ion is in the trivalent state and a quadrupole interaction exists in this compound. Both the magnetic susceptibility and the electron paramagnetic resonance (EPR) spectrum measurements show that the Gd^{3+} ion is in the $^8S_{7/2}$ state. In addition, the anisotropic EPR spectrum indicates that the six oxygen coordination around the Gd^{3+} ion has no longer a perfect octahedral symmetry. © 1999 Academic Press

INTRODUCTION

It is well known that complex oxides with perovskite-type structure often show functional properties (1, 2). Among them, we have paid attention to the $\text{Ba}_2\text{LnNbO}_6$ ($\text{Ln} = \text{lanthanide elements}$) compounds. They were first synthesized by Brixner (1) and were determined to have a cubic perovskite-type structure with the exception of $\text{Ln} = \text{La}$ which is a tetragonally distorted structure, and some of them have ferroelectric properties. Later, Filip'ev *et al.* (3) reported that the structure of $\text{Ln} = \text{La}$ had a rhombohedrally distorted structure. Anderson *et al.* (4), however, point out that the crystal system of $A_2\text{BB}'\text{O}_6$ double perovskites is cubic, orthorhombic, or monoclinic, because the $B(B')$ -cation arrangement is limited to be a random type, a rock salt type, or a layered type. When the $B(B')$ -cation arrangement is a rock salt type, the crystal system

should be either a cubic one ($Fm\bar{3}m$) or a monoclinic one ($P2_1/n$).

In order to clarify these discrepancies among them, we have prepared $\text{Ba}_2\text{LnNbO}_6$ ($\text{Ln} = \text{Y, La, Pr, Nd, Sm, Eu, Gd, Tb, Dy, Ho, Er, Tm, Yb, and Lu}$), carried out their X-ray diffraction measurements, and analyzed their crystal structures. In addition, magnetic susceptibility, electron paramagnetic resonance (EPR), and Mössbauer spectrum measurements have been performed for these compounds in the temperature range between 2 and 400 K to elucidate their electronic structures.

EXPERIMENTAL

1. Sample Preparation

Polycrystalline samples of $\text{Ba}_2\text{LnNbO}_6$ were prepared by a standard ceramic technique. As starting materials, barium carbonate BaCO_3 , lanthanide sesquioxide Ln_2O_3 ($\text{Ln} = \text{Y, La, Nd, Sm, Eu, Gd, Dy, Ho, Er, Tm, Yb, and Lu}$), and diniobium pentaoxide Nb_2O_5 were used. For the case of Ce, Pr, and Tb, CeO_2 , Pr_6O_{11} , and Tb_4O_5 were used. These reagents were weighed in appropriate metal ratios and ground intimately in an agate mortar. The mixtures were pressed into pellets and then heated in air at 1300°C for 24 h. The pellets were reground, repressed, and heated in air at 1400°C for 24 h. These procedures were repeated several times.

2. X-Ray Diffraction and Magnetic Measurements

Powder X-ray diffraction (XRD) patterns were measured with $\text{CuK}\alpha$ radiation on a RINT2000 (Rigaku) diffractometer. XRD data were collected by step scanning over the range $10^\circ \leq 2\theta \leq 120^\circ$ in increments of 0.04° (2θ).

The structure refinement was carried out by Rietveld analysis for the XRD data with the RIETAN-97B program (5).

Magnetic susceptibilities were measured in a magnetic field of 0.1 T over the temperature range between 2 and 400 K with a SQUID magnetometer (Quantum Design, MPMS5S). The measurements were carried out under both zero-field-cooled condition (ZFC) and field-cooled condition (FC). The former was measured on heating the sample to 400 K after zero-field cooling to 2 K. The latter was measured on cooling the sample from 400 to 2 K at 0.1 T.

EPR measurements were made at room temperature using a JEOL-RE2X spectrometer operating at X-band frequency (~ 9.1 GHz). The magnetic field was swept up to 1.0 T.

The ^{151}Eu Mössbauer spectrum was measured with a conventional transmission Mössbauer spectrometer VT-6000 (Laboratory Equipment Co.) in the constant acceleration mode at room temperature. A source of up to 100 mCi of $^{151}\text{SmF}_3$ was used and the spectrometer was calibrated using EuF_3 at room temperature.

RESULTS AND DISCUSSION

Crystal Structure

The results of the X-ray diffraction measurements show that all the samples in this study except for $\text{Ba}_2\text{CeNbO}_6$ were formed in a single phase. The XRD data were indexed with a monoclinic unit cell. The diffraction profiles of all the compounds showed the existence of the super lattice reflection at $2\theta \approx 18^\circ$. Figure 1 shows the X-ray diffraction profile for $\text{Ba}_2\text{TmNbO}_6$, as an example. It is concluded that these compounds are ordered perovskites and their lattice parameters are double those of the single perovskite. We have

performed the Rietveld analysis for the XRD data. Table 1 lists the lattice parameters and the reliability factors for $\text{Ba}_2\text{LnNbO}_6$ prepared in this study. The atomic parameters for $\text{Ba}_2\text{PrNbO}_6$ after refinement are listed in Table 2. Since the atomic parameters for other compounds $\text{Ba}_2\text{LnNbO}_6$ are comparable with those for $\text{Ba}_2\text{PrNbO}_6$, we will not list them.

The structures were refined by applying the space group $P2_1/n$. This space group allows two crystallographically distinct octahedral sites in the perovskite structure, thus permitting 1:1 positional ordering between the *B* site ions, Ln^{3+} , and Nb^{5+} ions. These ions are arranging alternately and they have a rock salt sublattice. Figure 2 shows the crystal structure of $\text{Ba}_2\text{LnNbO}_6$.

Figure 3 shows the variation of lattice parameters for the $\text{Ba}_2\text{LnNbO}_6$ with the ionic radius of Ln^{3+} . As the atomic number of lanthanide ions increases (which means the decrease of ionic radius of Ln^{3+}), the lattice parameters, *a*, *b*, *c*', and the volume decrease. The parameter *c*' is $c/\sqrt{2}$. The parameter β increases with ionic radius of Ln^{3+} , indicating that from $\text{Ln} = \text{Lu}$ to La the crystal structures of $\text{Ba}_2\text{LnNbO}_6$ are more distorted from the cubic symmetry, due to the larger difference in ionic radius between *B* site ions, Ln^{3+} , and Nb^{5+} .

Figure 4 shows the variation of the average *Ln*-O and Nb-O bond lengths with the ionic radius of Ln^{3+} . The average *Ln*-O bond length increases with the ionic radius of Ln^{3+} . On the other hand, the average Nb-O bond length is nearly constant (~ 1.94 Å). This value is shorter than the Nb-O bond length calculated from using Shannon's ionic radii, 2.04 Å (6). This result indicates the existence of the covalency in the Nb-O bond in these $\text{Ba}_2\text{LnNbO}_6$ compounds.

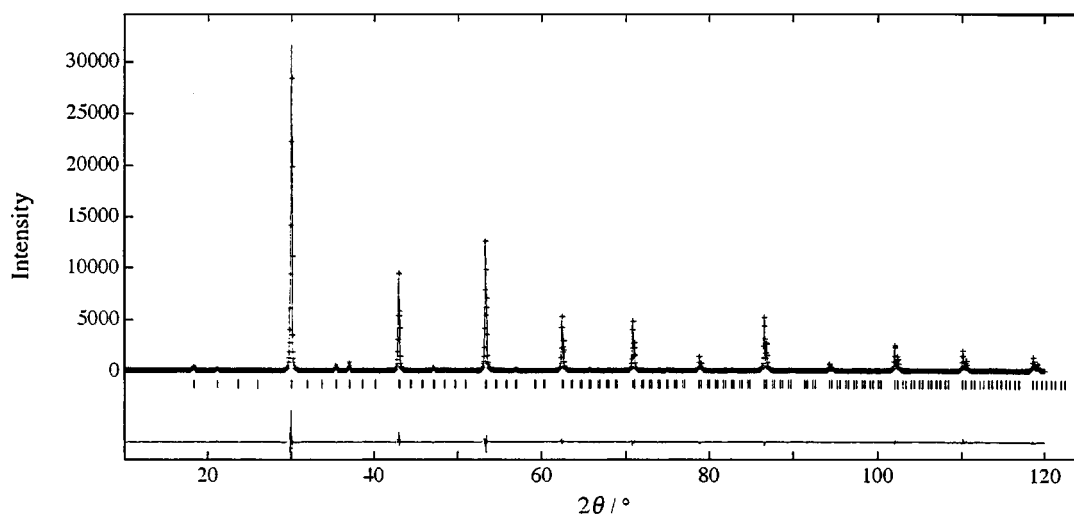


FIG. 1. Observed and calculated X-ray powder diffraction profiles for $\text{Ba}_2\text{TmNbO}_6$. The observed data are indicated by crosses and the calculated profile is the solid line. The short vertical lines below the profiles mark the positions of all possible Bragg reflections. The bottom continuous line is the difference between the observed and the calculated intensity.

TABLE 1
Unit Cell Parameters and R Factors for Ba_2LnNbO_6

Compound	a (Å)	b (Å)	c (Å)	β (°)	R_{wp}	R_1
Ba_2LaNbO_6	6.1407(1)	6.0899(1)	8.6031(2)	90.320(2)	12.30	2.65
Ba_2PrNbO_6	6.0913(1)	6.0539(1)	8.5509(2)	90.161(1)	12.25	3.74
Ba_2NdNbO_6	6.0764(1)	6.0437(1)	8.5365(2)	90.133(2)	12.48	2.54
Ba_2SmNbO_6	6.0187(4)	6.0156(4)	8.5355(3)	90.200(4)	11.94	2.92
Ba_2EuNbO_6	6.0035(4)	6.0043(3)	8.5242(3)	90.108(4)	12.53	2.37
Ba_2GdNbO_6	5.9962(5)	5.9961(4)	8.5119(2)	90.050(3)	12.31	3.32
Ba_2TbNbO_6	5.9845(4)	5.9838(3)	8.4820(2)	90.063(3)	12.20	2.37
Ba_2DyNbO_6	5.9752(7)	5.9751(7)	8.4610(2)	90.033(6)	13.40	2.80
Ba_2HoNbO_6	5.9653(5)	5.9644(4)	8.4396(4)	90.042(5)	12.79	3.37
Ba_2YNbO_6	5.9647(3)	5.9617(4)	8.4362(5)	90.017(7)	14.29	3.43
Ba_2ErNbO_6	5.9555(6)	5.9538(8)	8.4234(8)	90.020(8)	13.37	2.46
Ba_2TmNbO_6	5.9435(6)	5.9423(2)	8.4053(5)	90.041(7)	11.67	2.92
Ba_2YbNbO_6	5.9311(7)	5.9303(6)	8.3897(4)	90.026(8)	13.94	3.09
Ba_2LuNbO_6	5.9248(3)	5.9214(2)	8.3735(4)	90.015(9)	14.60	3.34

$$\text{Note. } R_{WP} = \left[\frac{\sum_k w_k [I_k(\text{obs}) - I_k(\text{calc})]^2}{\sum_k w_k I_k(\text{obs})^2} \right]^{1/2},$$

$$R_1 = \frac{\sum_k |I_k(\text{obs}) - I_k(\text{calc})|}{\sum_k I_k(\text{obs})}.$$

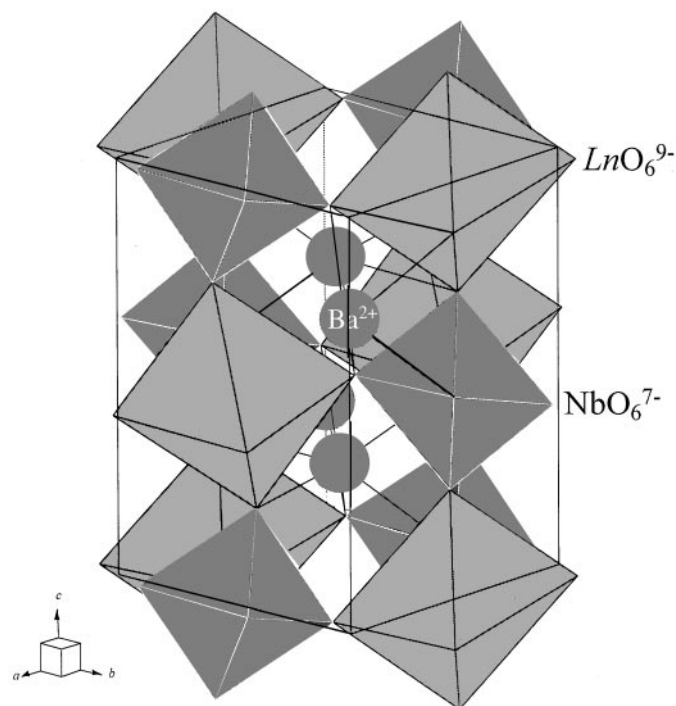
Magnetic Properties

The results of the magnetic susceptibility measurements for Ba_2LnNbO_6 show that they are paramagnetic down to 2 K. The electronic configuration of Nb^{5+} is $[Kr]4d^0$ ($[Kr]$, krypton core); i.e., this ion is diamagnetic. Therefore, the paramagnetic ion in the Ba_2LnNbO_6 is a Ln^{3+} ion. Their magnetic susceptibilities except for Ba_2SmNbO_6 and Ba_2EuNbO_6 followed the Curie law except at very low temperatures. Table 3 shows the effective magnetic moments of these compounds, μ_{exp} , and the calculated moments for the free Ln^{3+} ion, μ_{calc} . The effective magnetic moments obtained experimentally (μ_{exp}) in the temperature range of 250–400 K are in good agreement with the calculated values (μ_{calc}). This result indicates that the Ln^{3+} ions in the Ba_2LnNbO_6 are not affected by the crystal field.

In the following, we will discuss each of the magnetic behaviors of Ln^{3+} ions in these compounds.

TABLE 2
Atomic Positions and Isotropic Thermal Parameters for Ba_2PrNbO_6

Atoms	Sites	x	y	z	B (Å)
Ba	4e	0.0007(0.0014)	0.0019(0.0023)	0.2478(0.0008)	0.32
Pr	2d	0.5000	0.0000	0.0000	0.30
Nb	2c	0.5000	0.0000	0.5000	0.38
O(1)	4e	0.2062(0.0101)	0.2695(0.0124)	0.0035(0.0060)	0.80
O(2)	4e	0.2366(0.0122)	-0.2947(0.0108)	0.0013(0.0086)	0.71
O(3)	4e	-0.0467(0.0071)	0.5161(0.0193)	0.2278(0.0052)	0.73


FIG. 2. Crystal structure of Ba_2LnNbO_6 .

(a) Ba_2PrNbO_6 . The temperature dependence of magnetic susceptibility for Ba_2PrNbO_6 is shown in Fig. 5. It increases with decreasing temperature, but this increase does not become prominent in some temperature range. In this compound, the Pr^{3+} ion ($4f^2$) is coordinated by six oxygen ions with nearly octahedral symmetry. In the presence of an octahedral crystal field, the 3H_4 state of the Pr^{3+} ion (a nine-fold degenerate state) is split into a singlet (Γ_1), a doublet (Γ_3), and two triplets (Γ_4 and Γ_5) (7). Since the ground state of the Pr^{3+} ion is a singlet Γ_1 in this environment, the magnetic susceptibility of the Pr^{3+} ion should exhibit a temperature-independent behavior in a lower temperature region. We consider that an almost temperature-independent paramagnetic susceptibility found in the temperature region between 70 and 120 K (see Fig. 5) corresponds to this theoretical consideration. A sharp increase of magnetic susceptibility with decreasing temperature is observed at very low temperatures. This may be attributable to the paramagnetic behavior of Nb^{4+} ions (the electronic configuration is $[Kr]4d^1$) formed by the oxygen deficiency of this compound. It is known that some oxygen atoms are apt to be lacking in the perovskite oxides ABO_3 .

(b) Ba_2EuNbO_6 . The molar magnetic susceptibility of Ba_2EuNbO_6 as a function of temperature is shown in Fig. 6. Except at very low temperatures, the shape of this

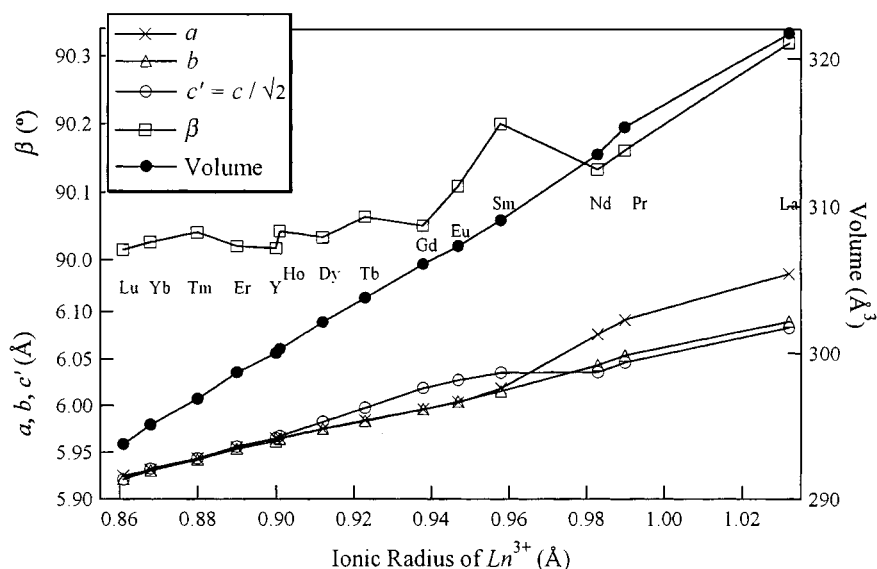


FIG. 3. Variation of lattice parameters for $\text{Ba}_2\text{LnNbO}_6$ with the ionic Ln^{3+} radius.

susceptibility vs the temperature curve is characteristic of a Van Vleck paramagnetism, with a constant susceptibility for the lower temperature range and a decreasing susceptibility with increasing temperature for $T \geq 100$ K.

The ground state 7F_0 of Eu^{3+} is nonmagnetic and the excited states 7F_J are close enough to give energy differences comparable to $k_B T$ (k_B , Boltzmann constant) at room temperature. Therefore, the magnetic susceptibility becomes independent of temperature in a lower temperature range. The molar magnetic susceptibility of the Eu^{3+} ion is expressed by the following equation (8),

$$\chi_M(\text{Eu}^{3+}) = \frac{0.12506}{\gamma T} \cdot \frac{24 + (13.5\gamma - 1.5)e^{-\gamma} + (67.5\gamma - 2.5)e^{-3\gamma} + (189\gamma - 3.5)e^{-6\gamma}}{1 + 3e^{-\gamma} + 5e^{-3\gamma} + 7e^{-6\gamma}}, \quad [1]$$

where $\gamma = \lambda/(k_B T)$ is the ratio of the multiplet width (the spin-orbital coupling constant, λ) and the thermal energy ($k_B T$). From the fitting of Eq. [1] to the experimental data, we have obtained $\lambda = 339 \text{ cm}^{-1}$. This value is reasonable as

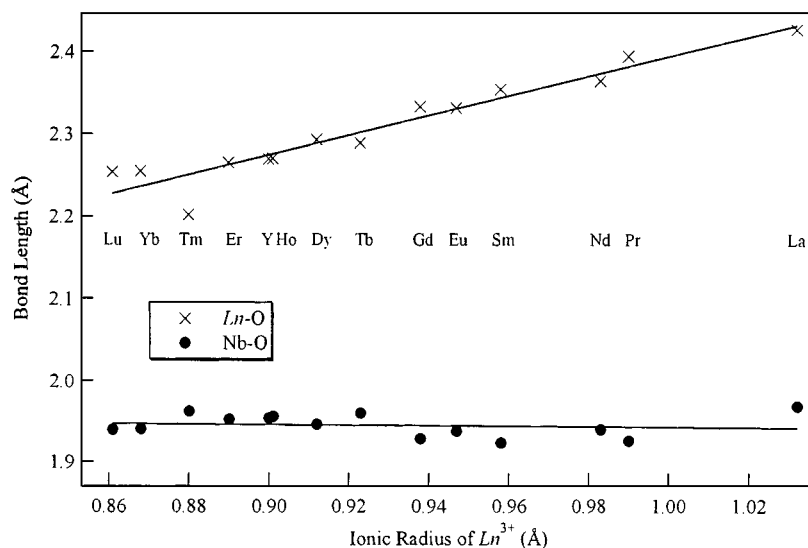


FIG. 4. Variation of Ln-O and Nb-O bond lengths with the ionic Ln^{3+} radius.

TABLE 3
The Experimental Magnetic Moments for Ln^{3+} (μ_{exp}) and the Calculated Magnetic Moments (μ_{calc}) for $\text{Ba}_2\text{LnNbO}_6$

Ln^{3+}	$\mu_{\text{exp}}/\mu_{\text{B}}$	$\mu_{\text{calc}}/\mu_{\text{B}}$
Pr^{3+}	3.45	3.58
Nd^{3+}	3.31	3.62
Gd^{3+}	7.96	7.94
Tb^{3+}	9.51	9.72
Dy^{3+}	9.93	10.63
Ho^{3+}	10.71	10.60
Er^{3+}	9.04	9.59
Tm^{3+}	7.22	7.57
Yb^{3+}	4.47	4.54

the spin-orbit coupling constant for Eu^{3+} ions in solids and it is comparable with 364 cm^{-1} for $\text{Ba}_2\text{EuIrO}_6$ (9) and 340 cm^{-1} for $\text{Sr}_2\text{EuIrO}_6$ (10). A paramagnetic behavior found in this compound at very low temperatures may be also attributable to the Nb^{4+} ions formed due to the oxygen deficiency.

The ^{151}Eu Mössbauer spectrum of $\text{Ba}_2\text{EuNbO}_6$ compound was measured at room temperature (Fig. 7). The Eu site in this $\text{Ba}_2\text{EuNbO}_6$ (space group, $P2_1/n$) has the point symmetry $\bar{1}$. It is known that an electric field gradient tensor exists in this point symmetry (11). Therefore, a nonzero quadrupole interaction is expected at the Eu site. The quadrupole interaction is given by

$$H_Q = \frac{e^2qQ}{4I(2I-1)} [3I_z^2 - I(I+1) + \eta(I_x^2 - I_y^2)], \quad [2]$$

where I is the nuclear spin, Q is the quadrupole moment, $eq = V_{zz}$, and $\eta = (V_{xx} - V_{yy})/V_{zz}$ (V_{ii} is the electric field gradient tensor) (12). Since the point symmetry $\bar{1}$ is not axially symmetric, the asymmetry parameter $\eta \neq 0$ in Eq. [2]. The observed spectrum exhibits a slightly asymmetric line (see Fig. 7). It is impossible to fit such a spectrum with a single Lorentzian line, because of the distortion due to a quadrupole interaction. As shown in Fig. 8, 12 possible transitions due to the quadrupole interaction should be considered in analyzing this Mössbauer spectrum. The spectrum is, therefore, fitted with 12 Lorentzian lines (13). The ^{151}Eu Mössbauer parameters, the isomer shift δ , the quadrupole coupling constant $eV_{zz}Q_g$, and the asymmetry parameter η were determined (Table 4). The following numerical values were adopted in this study: $R_Q = 1.312$ (the ratio of the excited and ground state quadrupole moments, Q_e/Q_g) and $Q_g = 1.14$ (14). It is noted that the Eu ions are in the trivalent state from the value of the isomer shift δ (1.50 mm/sec) (15). Since the quadrupole coupling constant ($eV_{zz}Q_g$) and the asymmetry parameter (η) were determined to be 4.96 mm/sec and 0.35, respectively, the quadrupole coupling interaction exists in this $\text{Ba}_2\text{EuNbO}_6$ compound. It is, therefore, confirmed that the electric field gradient at the Eu nuclei exists. The quadrupole coupling constant is positive in this case. This is the same result as those for $\text{Ba}_2\text{EuIrO}_6$ (4.92 mm/sec) and $\text{Sr}_2\text{EuIrO}_6$ (3.39 mm/sec) (9).

(c) $\text{Ba}_2\text{GdNbO}_6$. The magnetic susceptibility of $\text{Ba}_2\text{GdNbO}_6$ follows the Curie law, i.e., its reciprocal susceptibility vs temperature curve is fitted well with a straight

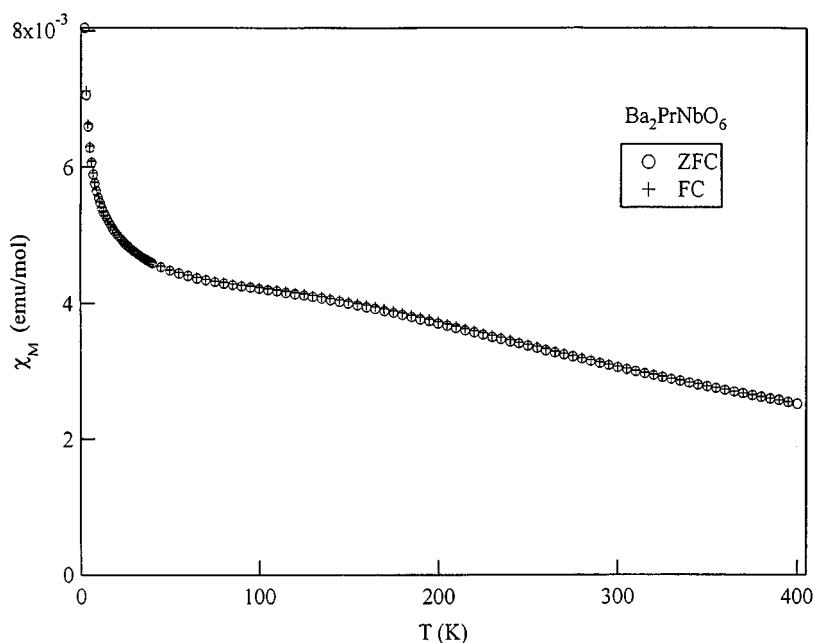


FIG. 5. Magnetic susceptibility vs temperature for $\text{Ba}_2\text{PrNbO}_6$.

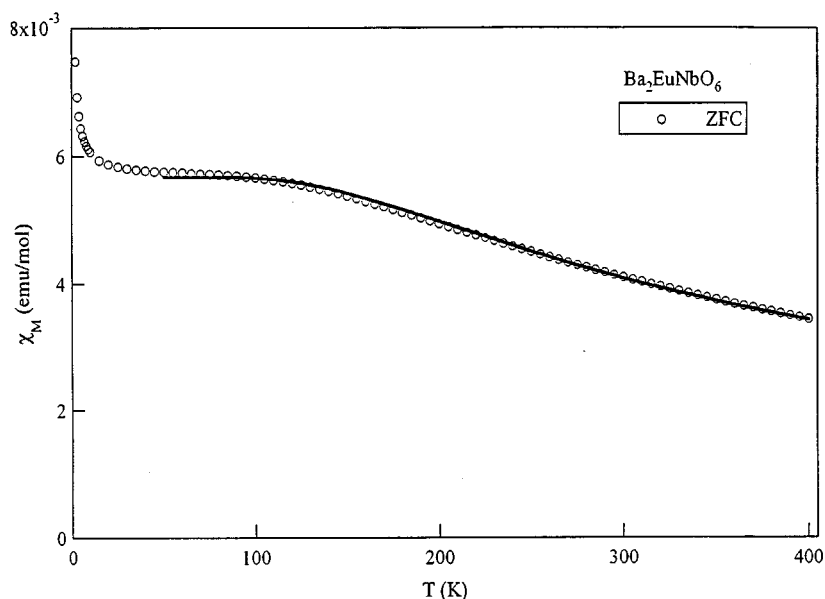


FIG. 6. Magnetic susceptibility vs temperature for $\text{Ba}_2\text{EuNbO}_6$. The solid line is calculated with Eq. [1] in the temperature range of 50–400 K.

line. This property is characteristic of the ground state of $^8S_{7/2}$. The effective magnetic moment of the Gd^{3+} ion is determined to be $7.96 \mu_B$ from this susceptibility measurement.

Figure 9 shows the X-band EPR spectrum for Gd^{3+} ion ($4f^7$) in $\text{Ba}_2\text{GdNbO}_6$ measured at room temperature. A single broad line centered at the magnetic field 3278 G was observed. The effective magnetic moment of the Gd^{3+} ion is calculated to be $7.87 \mu_B$ from EPR data ($g = 1.98$). Both the effective magnetic moments of the Gd^{3+} ion deter-

mined from the magnetic susceptibility and the EPR measurements are in good agreement with the calculated magnetic moment ($7.94 \mu_B$), which means that the ground state of the Gd^{3+} ion in $\text{Ba}_2\text{GdNbO}_6$ is a pure $^8S_{7/2}$ state. The anisotropic spectrum indicates that the six oxygen coordination around the Gd^{3+} ion has no longer a perfect octahedral symmetry.

(d) $\text{Ba}_2\text{YbNbO}_6$. Figure 10 shows the temperature dependence of magnetic susceptibility measured for

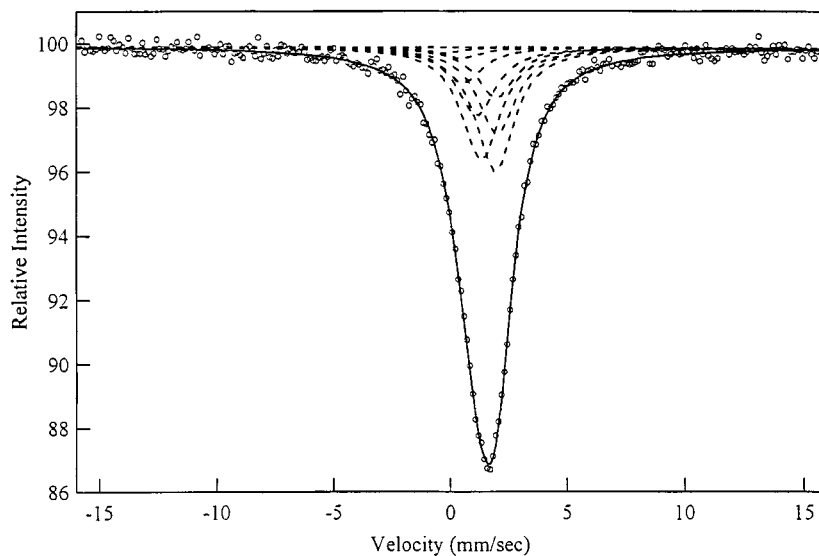


FIG. 7. ^{151}Eu Mössbauer spectrum of $\text{Ba}_2\text{EuNbO}_6$ at room temperature. The solid line is a calculated line with 12 Lorentzians.

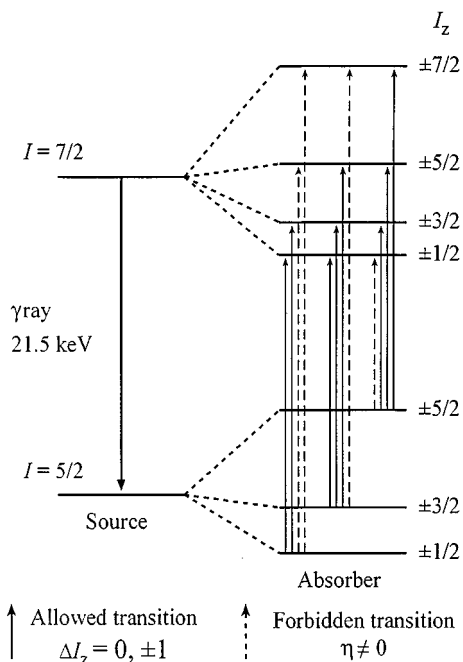


FIG. 8. Twelve possible transitions by a quadrupole interaction of ¹⁵¹Eu nucleus.

Ba₂YbNbO₆. When an Yb³⁺ ion (4f¹³) exists in the octahedral crystal field, the ground state ²F_{7/2} of the Yb³⁺ ion is split into two doublets (Γ₆ and Γ₇) and one quartet (Γ₈). The ground state is Γ₆ (7). The magnetic susceptibility is given by the following equation (16),

$$\chi_M(\text{Yb}^{3+}) = \frac{N_A g_J^2 \mu_B^2 J(J+1)}{3k_B T}.$$

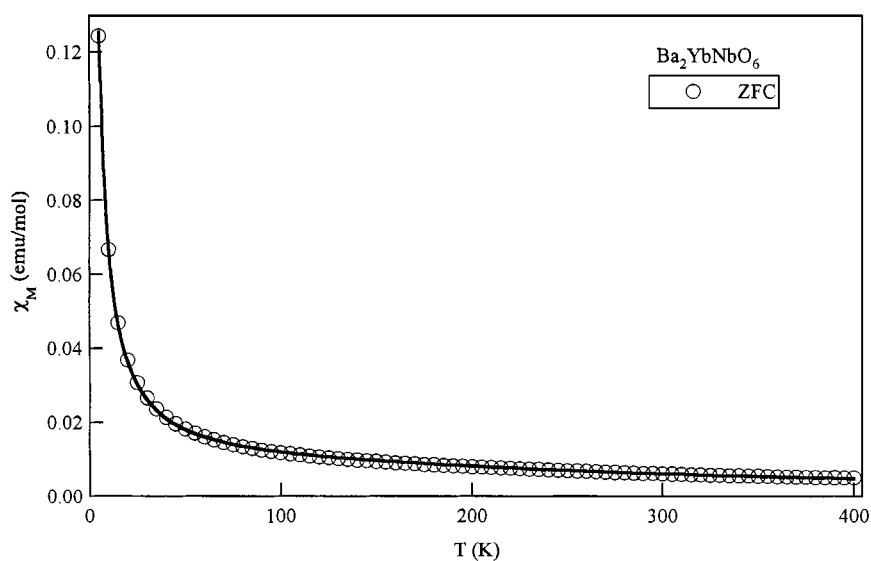


FIG. 10. Measured (○) and calculated (solid line) magnetic susceptibility for Ba₂YbNbO₆.

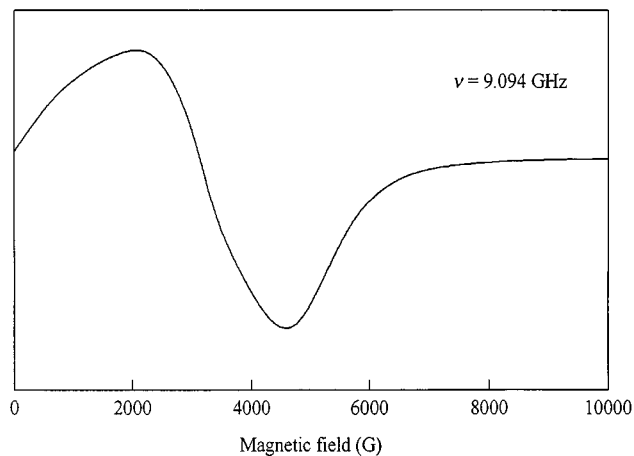


FIG. 9. EPR spectrum of Gd³⁺ in Ba₂GdNbO₆ at room temperature.

$$\frac{98 + 260e^{-b} + 162e^{-a} + 432(e^{-b} - e^{-a})/(a-b) + 560(1 - e^{-b})/b}{378(1 + 2e^{-b} + e^{-a})}, \quad [3]$$

where $a = \Delta_{67}/(k_B T)$ and $b = \Delta_{68}/(k_B T)$; Δ is the energy difference between the Γ₆ ground state and the Γ₇ or Γ₈ excited state. By fitting Eq. [3] to the experimental susceptibility data, we have obtained $\Delta_{67} = 1058 \text{ cm}^{-1}$, $\Delta_{68} = 368 \text{ cm}^{-1}$, and $\mu_{\text{exp}} = 4.30 \mu_B$. This effective magnetic moment of Yb³⁺ experimentally determined is a little smaller than the free ion value (4.54 μ_B), which means the Yb³⁺ ion in Ba₂YbNbO₆ is slightly affected by the crystal field.

TABLE 4
¹⁵¹Eu Mössbauer Parameters of Ba₂EuNbO₆

δ (mm/sec)	$eV_{zz}Q_g$ (mm/sec)	η
1.50	4.96	0.35

Note. δ , $eV_{zz}Q_g$, and η are isomer shift, quadrupole coupling constant, and asymmetry parameter, respectively.

REFERENCES

1. L. Brixner, *J. Inorg. Nucl. Chem.* **15**, 352 (1960).
2. M. Tanaka and K. Kageyama, *J. Am. Ceram. Soc.* **72**, 1955 (1989).
3. V. S. Filip'ev and E. G. Fesenko, *Kristallografiya* **6**, 770 (1961).
4. M. T. Anderson, K. B. Greenwood, G. A. Taylor, and K. R. Poeppelmeier, *Prog. Solid State Chem.* **22**, 197 (1993).
5. F. Izumi, in "The Rietveld Method" (R. A. Young, Ed.), Chap. 13. Oxford Univ. Press, Oxford, 1993.
6. R. D. Shannon, *Acta Crystallogr. Sect. A* **32**, 751 (1976).
7. K. R. Lea, M. J. M. Leask, and W. P. Wolf, *J. Phys. Chem. Solids* **23**, 1381 (1962).
8. J. H. Van Vleck, "The Theory of Electric and Magnetic Susceptibilities." Oxford Univ. Press, London, 1931.
9. M. Wakeshima, D. Harada, Y. Hinatsu, and N. Masaki, *J. Solid State Chem.* **147**, 618 (1999).
10. D. Harada, M. Wakeshima, and Y. Hinatsu, *J. Solid State Chem.* **145**, 356 (1999).
11. P. Gülich, R. Link, and A. Trautwein, in "Inorganic Chemistry Concepts," Vol. 3. Springer-Verlag, Berlin, 1978.
12. C. P. Slichter, "Principles of Magnetic Resonance." Harper & Row, New York, 1963.
13. G. K. Shenoy and B. D. Dunlap, *Nucl. Instrum. Methods* **71**, 285 (1969).
14. J. G. Stevens, in "Handbook of Spectroscopy" (J. W. Robinson, Ed.), Vol. III, p. 464, CRC Press, Boca Raton, FL, 1981.
15. E. R. Bauminger, G. M. Kalvius, and I. Nowik, in "Mössbauer Isomer Shifts" (G. K. Shenoy and F. E. Wagner, Eds.), p. 661. North-Holland, Amsterdam, 1978.
16. B. D. Dunlap and G. K. Shenoy, *Phys. Rev. B* **12**, 2716 (1975).